JACS
JOURNAL OF THE AMERICAN CHEMICAL SOCIETY

COMMUNICATION

pubs.acs.org/JACS

Highly Efficient Catalytic Microengines: Template Electrosynthesis of Polyaniline/Platinum Microtubes

Wei Gao, Sirilak Sattayasamitsathit, Jahir Orozco, and Joseph Wang*

Department of Nanoengineering, University of California, San Diego, La Jolla, California 92093, United States

Supporting Information

ABSTRACT: Highly efficient catalytic microtubular engines are synthesized rapidly and inexpensively using an electrochemical growth of bilayer polyaniline/platinum microtubes within the conically shaped pores of a polycarbonate template membrane. These mass-produced microtubular engines are only 8 μm long, are self-propelled at an ultrafast speed (of over 350 body lengths s^{-1}), and can operate in very low levels of the hydrogen peroxide fuel (down to 0.2%). The propulsion characteristics and optimization of these microtubular engines are described, along with their efficient operation in different biological environments which holds great promise for biomedical applications.

Synthetic nanoscale motors represent one of the most exciting challenges facing nanotechnology and hold considerable promise for diverse future applications.[1−5] Particular recent attention has been given to self-propelled, chemically powered catalytic nanomotors capable of converting energy into movement and forces.[1−5] Among these chemically powered nanomotors, catalytic microtube engines—pioneered by Mei and Schmidt[5−7]—are particularly attractive for practical applications due to their efficient bubble-induced propulsion in relevant biological fluids and salt-rich environments.[8−10] The oxygen-bubble propulsion mechanism of tubular microengines, associated with their conical shape and inner Pt surface, thus addresses the ionic-strength limitation and the limited scope of catalytic nanowire motors.[11] Such powerful microengines are commonly prepared by top-down photolithography, e-beam evaporation, and stress-assisted rolling of functional nanomembranes on polymers into conical microtubes. While they offer an extremely attractive performance, their practical utility is greatly hindered by the complexity of the fabrication process and related (clean-room) costs. Another approach for preparing microengines, involving sequential electrodeposition of platinum and gold layers onto an etched silver wire template,[12] offers a low yield and inferior propulsion behavior.

Here we demonstrate a greatly simplified membrane-templated mass production of high-performance catalytic microtubular engines. The resulting microtubes have significantly smaller size than commonly used rolled-up microengines (8 vs 50—100 μm), require very low fuel concentrations (down to 0.2% H_2O_2 vs 1.5%), and move at a very high speed (over 350 body lengths s^{-1}). The template electrodeposition method has been widely used for preparing different types of nanowires[13] and is commonly employed for preparing bimetallic catalytic nanowire motors.[2,3] To realize the synthesis of efficient conical microtube engines, we relied here on a unique combination of commercial microporous membranes, containing a huge number of uniform double-conical pores (Whatman Catalog No. 7060-2511), plated with polymeric/metal bilayers with a highly catalytic inner platinum surface. Martin[14] and Whitesides[15] demonstrated the successful template synthesis of cylindrical conducting-polymer microtubes, while Wan and Bai[16] described the template preparation of Sn/Pt bimetallic nanotubes based on evaporation and electrodeposition methods. Template electrosynthesis of microstructures of different shapes, including conical and double-conical nanowires and microtubes, was also described[17,18] but not in connection to nanomotors.

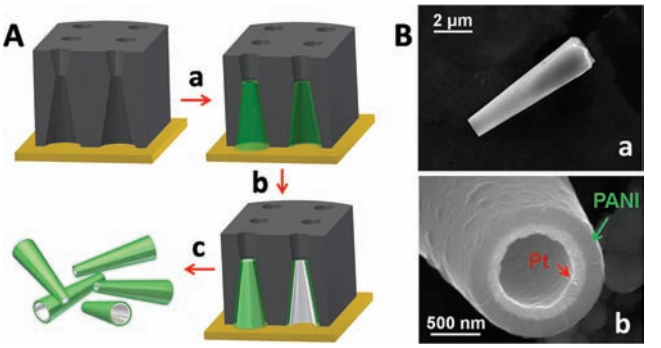

Figure 1. (A) Preparation of bilayer PANI/Pt microtubes using Cyclopore polycarbonate membranes: (a) deposition of the polyaniline (PANI) microtube, (b) deposition of the Pt microtube, and (c) dissolution of the membrane and release of the bilayer microtubes. (B) SEM images of the microtube engines: (a) side view and (b) cross view of a bilayer PANI/Pt microtube.

Figure 1A depicts the process of template preparation of polyaniline (PANI)/platinum bilayer microtubular engines. The template used in this process is a commercially available 20-μm-thick Cyclopore polycarbonate membrane, which has a symmetrical double-cone pore structure of 2 μm diameter on both sides and 1 μm in its center. By using one portion of the double cone (Figure 1A), such a membrane provides an attractive asymmetric template structure, as required for the bubbling propulsion mechanism. Due to solvophobic and electrostatic effects,[14] aniline monomers initially polymerize on the inner wall of the membranes, leading to a rapid formation of a PANI film. A platinum tube layer is subsequently plated inside the PANI tube using a galvanostatic method. The resulting conical bilayer microtube structure is preserved after the template dissolution.

Received: April 24, 2011
Published: July 13, 2011

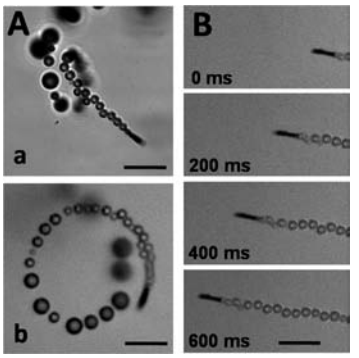

Figure 2. (A) Highly efficient tubular catalytic PANI/Pt microengines: spiral (a) and circular (b) motion. Trajectories are visualized by microbubble tails in a 1% H_2O_2 solution. (B) Time-lapse images (200 ms intervals) of the motion of a PANI/Ni/Pt trilayer microengine under a magnetic field in the presence of 1% H_2O_2 solution. Sodium cholate levels, 0.33% (w/v); scale bars, 20 μm.

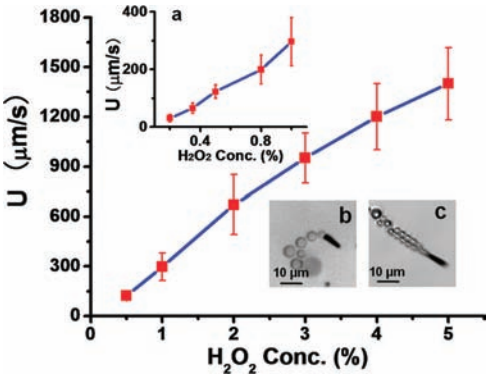

Figure 3. Dependence of the PANI/Pt microengine speed upon the hydrogen peroxide concentration over the 0.2−5.0% range, in the presence of 1.6% (w/v) sodium cholate (n = 60). Inset a), speed profile over the 0.2−1.0% peroxide range. Insets (b) and (c): propulsion in the presence of 0.3% and 0.5% hydrogen peroxide, respectively.

Figure 1B shows side-view (a) and cross-view (b) SEM images of a typical 8-μm-long conical microtube. The PANI/Pt bilayer tube has a defined geometry with outer diameters of 2 and 1.1 μm, along with inner openings of 1.5 and 0.5 μm, and a taper angle of 3.2°. The PANI and Pt layers are easily visualized from the cross-view image, with a thickness of 180 and 80 nm, respectively. Common rolled-up microengines have significantly larger openings of 5−10 μm in diameter.[5−7] An EDX mapping analysis, carried out to confirm the bilayer content (e.g., Supporting Information, SI Figure 1b,c), shows clearly the presence of both platinum and carbon (from PANI) within the conical microtube.

The high propulsion power of the template-prepared PANI/Pt microtube engines is illustrated in Figure 2 and its corresponding videos. For example, Figure 2A(a,b) and SI Videos 1 and 2 show the movement of two microengines in a 1% H_2O_2 solution (containing 0.33% of the sodium cholate surfactant) during a 3 s period. The two microengines move rapidly in spiral and circular trajectories, with an average speed of 120 μm s^{-1}. Similar motion trajectories were reported for larger rolled-up microengines.[7] Long oxygen bubble tails, released from the wider tubular openings, can be easily visualized, with individual microbubbles of 2.5 μm. While the bilayer microengines of Figure 2A move randomly, it is also possible to guide them magnetically by depositing an intermediate ferromagnetic Ni layer and forming a trilayer PANI/Ni/Pt microengine. Figure 2B shows time-lapse images (200 ms intervals) of the motion of a PANI/Ni/Pt microengine under a magnetic field in the presence of 1% H_2O_2 solution. The corresponding SI Video 3 illustrates the magnetically guided directional motion of one PANI/Ni/Pt microengine. The speed of the trilayer microengine decreases to 80 μm s^{-1}, compared to 120 μm s^{-1} for the bilayer PANI/Pt microtubes (under the same conditions), reflecting the smaller pore diameter associated with the Ni layer. Our further experimental results show that the opening size of PANI/Pt microengines has a profound effect on their speed. For example, reducing the inner opening diameter from 500 to 150 nm (measured from the smaller side of the tube) resulted in a lower speed of 60 μm s^{-1} (vs 120 μm s^{-1} using 1% H_2O_2 and 0.33% sodium cholate).

The concentration of hydrogen peroxide fuel strongly influences the velocity of the catalytic microengines. As illustrated in Figure 3, the average speed of the PANI/Pt microtubular engines increases from 123 ± 21.4 μm s^{-1} (15 body lengths s^{-1}) at 0.5% H_2O_2 to 1410 ± 172 μm s^{-1} (~180 body lengths s^{-1}, see SI Video 4) at 5% H_2O_2 (using 1.6% sodium cholate surfactant; n = 60). The greatly increased speed of the PANI/Pt microengines over the entire range of H_2O_2 fuel (0−5%) reflects the higher pressure experienced by the bubbles.[7] However, using a low peroxide level (below 5%), the template bilayer microengines display a much faster speed than the rolled-up microengines.[7,20] The fastest observed speed of the microengines exceeds 3 mm s^{-1}, i.e., more than 375 body lengths s^{-1}, as illustrated in SI Video 5 in connection to 10% H_2O_2 and 1.6% sodium cholate. Such ultrafast speed is attributed primarily to increased electrocatalytic reactivity of the inner platinum surface, associated with the higher surface roughness [Figure 1B(b)] compared to the smooth platinum surface of rolled-up microengines. Increasing the area of Pt electrode sensors was shown previously to increase their catalytic reactivity toward the decomposition of hydrogen peroxide.[21] Our experiments also show that such microengines can move in very low peroxide levels. Inset (a) of Figure 3 shows the dependence of the microengine speed upon the hydrogen peroxide concentration over the 0.2−1.0% range. Well-defined propulsion is observed over this range of low peroxide concentrations, with speed ranging between 25 and 285 μm s^{-1}. For example, SI Video 6 displays a typical microtube movement of ~25 μm s^{-1} (over 3 body length s^{-1}) in a 0.2% H_2O_2 solution. Even further lowering of the peroxide concentration to 0.05% can be achieved by adding 0.05% hydrazine (e.g., SI Video 7). In contrast, the lowest peroxide level reported for propelling catalytic rolled-up microengines is 1.5% (resulting in a low speed of 1 body length s^{-1}).[19]

The radius and frequency of the generated oxygen bubbles are influenced by the level of peroxide fuel. Insets (b) and (c) of Figure 3 illustrate the representative bubble size of microtubular engines in the presence of 0.3 and 0.5% H_2O_2, respectively, and 1.6% (w/v) sodium cholate surfactant. The bubble frequency increases greatly (from 16 to 60 Hz) upon raising the peroxide level from 0.3 to 0.5%, while the bubble size decreases from 2.6 to 2.0 μm. As expected,[7] larger bubbles with a lower frequency led to a lower speed (e.g., 40 μm s^{-1} in 0.3% hydrogen peroxide as compared to 120 μm s^{-1} in 0.5% H_2O_2). We also observed that the average moving steps are close to the bubble radius. For example, in 0.5% hydrogen peroxide—where the bubble radius is

around 2 μm and the frequency around 60 Hz—the microengine speed is 122 μm s^{-1}, i.e., nearly corresponding to the product of the bubble radius and frequency, indicating that the drag forces on the engines and bubbles are comparable. Similar effects were reported for the rolled-up microtubes.[7]

The influence of surfactant concentration (sodium cholate in this paper) on the speed of microengines was also examined (SI Figure 2). Increased speed is observed upon raising the surfactant concentration over the 0−5% range. Using a 1% H_2O_2 solution containing 0.33% sodium cholate, the microengines have an average speed of 120 μm s^{-1}; the speed increases to around 300 μm s^{-1} in 1.6% sodium cholate and to 520 μm s^{-1} in 5% sodium cholate. In the presence of 2% H_2O_2 (along with 5% sodium cholate), the microengines move at 1.0 mm s^{-1}. This surfactant-induced increase of the speed is attributed to the lowering of the surface tension, smaller bubble size, and a much higher bubble frequency, in a manner analogous to those reported for rolled-up microrockets.[6,7]

Common catalytic nanowire motors operate only in low-ionic-strength aqueous solutions[11] and hence cannot be applied to realistic biological environments. Microtubular engines address this ionic-strength limitation and can expand the scope of nanomotors to salt-rich environments.[9,10,12] For example, SI Figure 3A,B (corresponding to SI Videos 8 and 9) illustrates the movement of the template-prepared microengine in realistic biological environments, such as cell culture media and human serum, respectively (containing 1.5% H_2O_2 and 2% sodium cholate). The new microengines propel efficiently using physiological conditions, with high average speeds of 150 (cell culture) and 95 (serum) μm s^{-1}. The decrease of the speed (vs more than 300 μm s^{-1} in water under similar conditions) is attributed to viscosity effects (e.g., ∼1.5 mPa·s for human serum). A slower speed (∼200 μm s^{-1}) was also observed in a high ionic aqueous solution (3 M NaCl, viscosity ∼1.2 mPa·s).

Assuming the microengine as a cylinder microrod (since the fluid cannot freely flow through microengine because of the oxygen bubbles), 8 μm in length and 2 μm in diameter, moving at a speed of 1400 μm s^{-1}, we can roughly estimate the drag force by using Stokes's drag theory,

$$F_d = \frac{2\pi\mu LU}{\ln(L/a) - 1/2}$$

where F_d is the fluid resistance, U is the speed in the microengine, μ is the fluid dynamic viscosity, and L and a are the length and radius of the microtubes, respectively. The estimated drag force of the microengines, 45 pN, is sufficient for transporting large cargos such as cells.[8,9,20]

In conclusion, we demonstrated that remarkably efficient microtube engines can be mass-produced by a greatly simplified, low-cost membrane template electrodeposition. The resulting PANI/Pt microtubes are significantly smaller than rolled-up microengines, move at a much higher speed (>350 body lengths s^{-1}), and require very low fuel concentrations. Reducing the peroxide level leads to greatly improved cell viability for relevant biomedical applications.[9] While the concept has been illustrated in connection to PANI/Pt microengines, the template electrodepostion allows plating of different outer or inner layer materials (polymers, metals, etc.) to meet specific needs and different applications, and expanding the scope of catalytic micro/nanomachines. The attractive properties of these new template-prepared microtube engines, along with their bioenvironmental compatibility, hold considerable promise for the design of practical nanomachines for a wide range of important future applications.

■ ASSOCIATED CONTENT

Supporting Information. Microengine preparation, related protocols, instrumentation, reagents, additional data, and SI Videos 1−9. This material is available free of charge via the Internet at http://pubs.acs.org.

■ AUTHOR INFORMATION

Corresponding Author
josephwang@ucsd.edu

■ ACKNOWLEDGMENT

This work was supported by the National Science Foundation (Award No. CBET 0853375). S.S. was supported by DOE BES DE-SC0004937. J.O. acknowledges a Beatriu de Pinós postdoctoral fellowship from the Government of Catalonia. The authors thank A. Pei, A. Ponedal, and B. Chuluun for their help.

■ REFERENCES

(1) Mirkovic, T.; Zacharia, N. S.; Scholes, G. D.; Ozin, G. A. *ACS Nano* **2010**, *4*, 1782–1789.
(2) Wang, J. *ACS Nano* **2009**, *3*, 4–9.
(3) Mallouk, T. E.; Sen, A. *Sci. Am.* **2009**, *300*, 72–77.
(4) Ebbens, S. J.; Howse, J. R. *Soft Matter* **2010**, *6*, 726–738.
(5) Mei, Y. F.; Solovev, A. A.; Sanchez, S.; Schmidt, O. G. *Chem. Soc. Rev.* **2011**, *40*, 2109–2119.
(6) Mei, Y. F.; Huang, G. S.; Solovev, A. A.; Urena, E. B.; Monch, I.; Ding, F.; Reindl, T.; Fu, R. K. Y.; Chu, P. K.; Schmidt, O. G. *Adv. Mater.* **2008**, *20*, 4085–4090.
(7) Solovev, A. A.; Mei, Y. F.; Urena, E. B.; Huang, G. S.; Schmidt, O. G. *Small* **2009**, *5*, 1688–1692.
(8) Sanchez, S.; Solovev, A. A.; Schulze, S.; Schmidt, O. G. *Chem. Commun.* **2011**, *47*, 698–700.
(9) Balasubramanian, S.; Kagan, D.; Hu, C.-M.; Campuzano, S.; Lobo-Castañon, M. J.; Lim, N.; Kang, D. Y.; Zimmerman, M.; Zhang, L.; Wang, J. *Angew. Chem., Int. Ed.* **2011**, *50*, 4161–4164.
(10) Kagan, D.; Campuzano, S.; Balasubramanian, S.; Kuralay, F.; Flechsig, G. U.; Wang, J. *Nano Lett.* **2011**, *11*, 2083–2087.
(11) Paxton, W. F.; Sundararajan, S.; Mallouk, T. E.; Sen, A. *Angew. Chem., Int. Ed.* **2006**, *45*, 5420–5429.
(12) Manesh, K. M.; Yuan, R.; Clark, M.; Kagan, D.; Balasubramanian, S.; Wang, J. *ACS Nano* **2010**, *4*, 1799–1804.
(13) Hurst, S. J.; Payne, E. K.; Qin, L. D.; Mirkin, C. A. *Angew. Chem., Int. Ed.* **2006**, *45*, 2672–2692.
(14) Parthasarathy, R. V.; Martin, C. R. *Chem. Mater.* **1994**, *6*, 1627–1632.
(15) Lahav, M.; Weiss, E. A.; Xu, Q.; Whitesides, G. M. *Nano Lett.* **2006**, *6*, 2167–2171.
(16) Guo, Y. G.; Hu, J. S.; Zhang, H. M.; Liang, H. P.; Wan, L. J.; Bai, C. L. *Adv. Mater.* **2005**, *17*, 746–750.
(17) Chakarvarti, S. K.; Vetter, J. *Radiat. Meas.* **1998**, *29*, 149–159.
(18) Li, N. C.; Yu, S. F.; Harrell, C. C.; Martin, C. R. *Anal. Chem.* **2004**, *76*, 2025–2030.
(19) Sanchez, S.; Solovev, A. A.; Mei, Y. F.; Schmidt, O. G. *J. Am. Chem. Soc.* **2010**, *132*, 13144–13145.
(20) Solovev, A. A.; Sanchez, S.; Pumera, M.; Mei, Y. F.; Schmidt, O. G. *Adv. Funct. Mater.* **2010**, *20*, 2430–2435.
(21) Evans, S. A. G.; Elliott, J. M.; Andrews, L. M.; Bartlett, P. N.; Doyle, P. J.; Denuault, G. *Anal. Chem.* **2002**, *74*, 1322–1326.